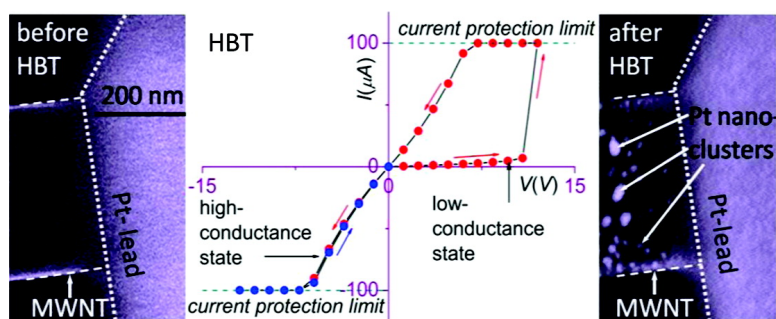


## Lu#ttinger Liquid to Al'tshuler#Aronov Transition in Disordered, Many-Channel Carbon Nanotubes

Swastik Kar, Caterina Soldano, Li Chen, Saikat Talapatra, Robert Vajtai, Saroj Nayak, and Pulickel M. Ajayan

ACS Nano, 2009, 3 (1), 207-212 • DOI: 10.1021/nn800678v • Publication Date (Web): 11 December 2008

Downloaded from <http://pubs.acs.org> on January 30, 2009



### More About This Article

Additional resources and features associated with this article are available within the HTML version:

- Supporting Information
- Access to high resolution figures
- Links to articles and content related to this article
- Copyright permission to reproduce figures and/or text from this article

[View the Full Text HTML](#)

# Luttinger Liquid to Al'tshuler–Aronov Transition in Disordered, Many-Channel Carbon Nanotubes

Swastik Kar,<sup>†,\*</sup> Caterina Soldano,<sup>†,\*</sup> Li Chen,<sup>†</sup> Saikat Talapatra,<sup>\*</sup> Robert Vajtai,<sup>§</sup> Saroj Nayak,<sup>†</sup> and Pulickel M. Ajayan<sup>§</sup>

<sup>†</sup>Department of Physics, Applied Physics and Astronomy, Rensselaer Polytechnic Institute, Troy, New York 12180, <sup>‡</sup>Department of Physics, Southern Illinois University Carbondale, Carbondale, Illinois 62901, and <sup>§</sup>Department of Mechanical Engineering and Materials Science, Rice University, Houston, Texas 77006. <sup>‡</sup>These authors contributed equally.

The interplay of disorder and interactions in one-dimensional (1D) systems has been a topic of extreme importance in condensed matter physics<sup>1,2</sup> for decades. In this context, the Luttinger liquid (LL) model<sup>2</sup> has successfully explained charge transport in a variety of systems such as tunneling into quantum-Hall edge states,<sup>3</sup> nanowires,<sup>4</sup> and carbon nanotubes.<sup>5–7</sup> While the presence of disorder in Luttinger liquids (such as arc-discharge grown carbon nanotubes) can cause weak localization<sup>8,9</sup> at low temperatures, they are expected to completely localize within the length scale of the mean free path  $l_e$  without any *diffusive transport* regime<sup>1,2</sup> at zero temperature. However, recent predictions<sup>10</sup> suggest that electron–electron ( $e$ – $e$ ) interactions in *many-channel* LLs allow low-energy excitations to *diffuse* over length scales much larger than  $l_e$ , suppressing the conductance  $G$  at low temperatures following an Al'tshuler–Aronov (AA)<sup>11</sup> correction. In this regime,  $e$ – $e$  interactions can be expected to have a strong impact on coherent transport. In carbon nanotubes, recent works<sup>12,13</sup> have shown that coherent transport, quantified by the phase-coherence length  $L_\phi$ , is sensitive to the electronic structure. However, its behavior at different electronic energies has not been studied. Since low-energy conductance is suppressed predominantly by  $e$ – $e$  interactions, the question arises whether phase coherence is recovered at higher electronic energies. Most works have focused on “clean” nanotubes, and highly disordered template-grown multiwall nanotubes (MWNTs) have received very little attention.<sup>14,15</sup> Additionally, most sidewall-contacted MWNT de-

**ABSTRACT** We present a simple method to increase the conductance of individual template-grown carbon nanotubes contacted with platinum electrodes using a high-bias treatment process which decorates the nanotubes with Pt nanoclusters. The temperature dependence of conductance of the modified carbon nanotubes follows very closely a Luttinger-liquid to Al'tshuler–Aronov anomaly and reveals enhanced number of channels and decreased disorder-density compared to the pristine tubes. Low temperature magnetotransport shows evidence of Rashba spin–orbit coupling, usually absent in bare nanotubes, and a strong suppression of phase coherence at low electronic energies due to electron–electron interactions.

**KEYWORDS:** carbon nanotubes · metal decoration · 1D hybrid nanostructure · Luttinger liquid · Al'tshuler–Aronov · correlated electron systems · weak-localization · spin–orbit coupling

vices are unable to access sufficient number of walls<sup>16</sup> to approach the many-channel limit.<sup>10</sup> Hence, the above-mentioned issues remain experimentally untested, for which 1D-systems with tunable number of channels and disorder density are highly desirable. Further, surface decoration of these systems with heavy-metal nanoclusters has been recently predicted<sup>17</sup> to cause the development of strong spin–orbit (SO) coupling mechanisms, usually absent in bare carbon nanotubes, and demands experimental verification.

## RESULTS AND DISCUSSIONS

In this paper, we present a method to substantially increase the number of quantum channels in individual carbon nanotubes and tune their disorder density *via* a controlled high-bias treatment (HBT) procedure. The process decorates the nanotubes with Pt nanoclusters. Temperature dependence of conductance of these devices validates the recently predicted<sup>10</sup> LL-AA behavior. Our *ab initio* density functional theory (DFT) calculations suggest that charge

\*Address correspondence to kars@rpi.edu, csoldano@cemes.fr.

Received for review October 10, 2008 and accepted November 26, 2008.

Published online December 11, 2008. 10.1021/nn800678v CCC: \$40.75

© 2009 American Chemical Society

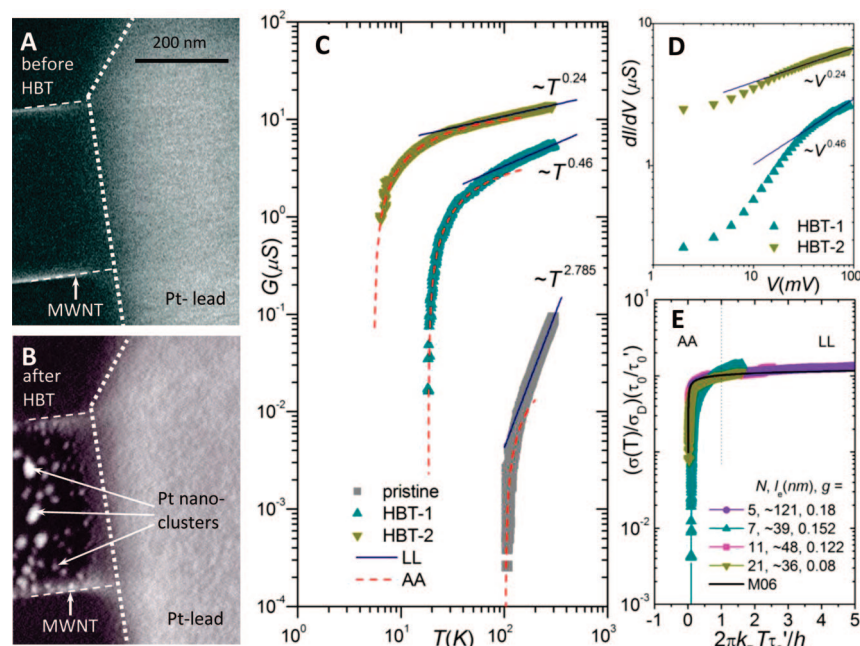


**Figure 1.** SEM images of a MWNT device near the contact region (A) before and (B) after an HBT process. Nanoclusters of platinum decorate the nanotube after the HBT process. (C) Temperature dependence of  $G$  in a pristine device, and after each step of two successive HBTs. The solid lines show Luttinger liquid (LL) fits in the higher  $T$  region and the dashed lines show the Al'tshuler-Aronov (AA) fits in the lower  $T$  region. (D) Bias dependence of  $dI/dV$  in HBT-modified devices at  $T = 7$  K, showing the LL power-law behavior at high biases (solid lines). (E) Renormalized conductivity  $(\sigma(T)/\sigma_0)(\tau_0/\tau_0')$  as a function of the scaled temperature  $T/T'$  calculated from  $G$  vs  $T$  curves of different devices. The corresponding values of  $N$ ,  $l_e$ , and  $g$  are also shown. The dark line (M06) shows digitized data from Figure 1 of Mora *et al.*<sup>26</sup>

transfer from platinum decorations on carbon nanotubes may provide part of the observed additional channels close to the Fermi level. These devices are highly correlated, and magnetoconductance measurements quantify the energy-dependence of decoherence at  $T = 7$  K. The magnetoconductance also contains small but distinct features which we attribute to SO scattering effects due to decoration of the nanotubes with platinum nanoclusters.

Two-terminal devices were fabricated using individual MWNTs of diameter  $d = 200$ – $250$  nm with platinum leads (separation  $L \approx 4$ – $5$   $\mu\text{m}$ ) attached by focused ion beam lithography (see Materials and Methods for more details). Devices were placed in a vacuum ( $p < 10^{-5}$  Torr) and current–voltage measurements were performed at room temperature with increasingly large biases. Sweeping-up to high biases ( $V > 10$  V) across the leads causes a sudden decrease in the device resistances by orders of magnitude. We refer to these as HBT-modified devices.<sup>18</sup> The application of a high bias across the high-resistance “pristine” devices generates sufficient local heating<sup>19</sup> and atomic migration<sup>20</sup> to substantially anneal defects and decorate the outer surface of the nanotube with metal nanoclusters migrating away from the contacts as seen in Figure 1A,B.

Previous reports on “clean” carbon nanotubes have demonstrated  $G(T) \propto T^\alpha$  for  $eV/k_B T \ll 1$ , and  $G(V) \propto V^\alpha$

for  $eV/k_B T \gg 1$ , including a universal scaling behavior<sup>8</sup>  $G(V,T)/T^\alpha = \int_{\text{LL}} [eV/k_B T]$ . However, investigations of disordered, few-channel nanotubes in the past remained from capturing the interplay of disorder and interactions in multichannel quantum wires, and most results have been interpreted in terms of weak-localization,<sup>9,10,21</sup> variable-range hopping,<sup>16</sup> two-wall conductance,<sup>17</sup> or environment-quantum-fluctuations.<sup>22</sup> Attempts to analyze our data in the framework of the above-mentioned mechanisms, or the finite-temperature effect of interaction-driven dephasing in single-channel disordered LLs,<sup>23</sup> were unsuccessful.

The pristine devices are highly disordered, with room-temperature resistances  $R_{296\text{K}} \approx$  tens of  $\text{M}\Omega$ . The HBT-modification dropped the  $R_{296\text{K}}$  down to a few tens of  $k\Omega$ . Figure 1C shows the temperature dependence ( $5 \text{ K} < T < 300 \text{ K}$ ) of low-bias (1 mV)  $G$  in a typical pristine device and after each step of two successive HBTs. The overall behavior in all our devices is a slow, power-law dependence of conductance  $G(T) \propto T^\alpha$  at higher  $T$ , with sharp suppression of

$G$  at lower  $T$ . In a multichannel LL, at higher temperatures  $T \gg T'$  (defined later),  $e$ – $e$  interactions renormalize the Drude conductivity to give a temperature dependence

$$\sigma(T) = Nv_F\tau_0 \frac{2e^2}{h} \left( \frac{2\pi}{e^{1.577}} \right)^\alpha \left( \frac{k_B T}{\hbar\omega_c} \right)^\alpha$$

where  $v_F$  is the Fermi velocity<sup>23</sup>  $\approx 8 \times 10^5 \text{ ms}^{-1}$ ,  $\tau_0$  is the elastic scattering time,  $\omega_c$  is the ultraviolet cutoff frequency, and  $N$  represents the number of LL channels. At lower temperatures ( $T \ll T'$ ), Al'tshuler–Aronov correction predicts a  $T$ -dependence,

$$\sigma(T) \approx Nv_F\tau_0 \frac{2e^2}{h} \left[ 1 - \frac{0.782\alpha}{1+g} \left( \frac{k_B T \tau_0'}{\hbar} \right)^{-1/2} \right]$$

where  $(\tau_0')^{-1}$  is the renormalized elastic scattering rate ( $\tau_0' = \tau_0(\omega_c\tau_0)^{-(\alpha/(\alpha+1))}$ ),  $g$  is the Luttinger parameter  $g = (1 + NU/\pi\hbar v_F)^{-1/2}$  and  $U$  represents the interaction potential.  $U > 0$  indicates increasing repulsive  $e$ – $e$  interactions, which drives  $g \rightarrow 0$ . Mora<sup>10</sup> *et al.* have recently given a unifying description (LL-AA model) of these two regimes, and the AA behavior was recently reported in highly disordered MWNTs.<sup>24</sup> Using the LL-AA model, independent fits for the high- and low-temperature regimes (shown with solid and dashed lines in Figure 1C) were used to analyze our data. At

**TABLE 1. Transport Properties Obtained from the LL-AA Fits for Two Devices Which Have Each Undergone Two HBT Cycles, HBT-1 and HBT-2, Respectively<sup>a</sup>**

	device 1 ( $L = 4.5 \mu\text{m}$ )			device 2 ( $L = 4.1 \mu\text{m}$ )		
	pristine	HBT-1	HBT-2	pristine	HBT-1	HBT-2
$\alpha$	2.785	0.46	0.24	2.2	0.16	0.15
$\sigma_D$ (S.m)	$2.1 \times 10^{-13}$	$2.1 \times 10^{-11}$	$5.8 \times 10^{-11}$	$3.6 \times 10^{-13}$	$4.1 \times 10^{-11}$	$4.7 \times 10^{-11}$
$N$	—	7	21	—	11	5
$l_e$ ( $10^{-9}$ m)	<2.7	39	36	<4.7	48	121
$Nl_e$ ( $10^{-9}$ m)	—	273	756	—	528	605
$L/l_e$	>1642	114	126	>872	85	34
$\omega_c$ ( $10^{13}$ s <sup>-1</sup> )	4.0	3.6	2.9	2.9	1.2	0.7
$\tau_0$ ( $10^{-15}$ s)	<3.4	49	45	<5.9	60	152
$\tau'_0$ ( $10^{-15}$ s)	<15	41	43	<20	63	152
$g$	—	0.152	0.08	—	0.122	0.179
$T'$ (K)	—	187	179	—	122	50

<sup>a</sup>Here,  $\sigma_D$  = Drude conductivity,  $\omega_c$  = ultraviolet cutoff frequency,  $N$  = number of channels,  $l_e$  = elastic mean free path,  $\tau_0$  = elastic mean free time,  $\tau'_0$  = renormalized elastic mean free time,  $g$  = Luttinger parameter,  $T' = [2\pi k_B \tau'_0 / h]^{-1}$  = LL-AA transition temperature.

higher temperatures, the pristine devices had large values of  $\alpha$  ( $2 < \alpha < 4$  for most devices), unexpectedly high for single LL channels, but possible for sequential *end–end* tunneling of electrons across multiple LLs.<sup>5</sup> Pristine devices were also found to have mean-free paths  $l_e$  ( $\approx \tau_0 v_F$ )  $< 5$  nm, and  $\tau_0 \approx 10^{-15}$  s, in agreement with that reported in ref 24. However, no self-consistent solution could be obtained for  $N \geq 1$ . Additionally, at the lowest measured  $T$ ,  $G$  showed no power-law dependence on the bias,  $V$  (not shown). Template-grown nanotubes have poor long-range graphitic order,<sup>25</sup> the charge-transport being *via* end–end tunneling between shorter graphene flakes. We conclude that pristine devices cannot be considered to be a continuous channel, but rather, a tunneling network of short length-scale LLs, with high disorder density ( $L/l_e \approx 10^3$ ). Table 1 summarizes some of the transport properties in our devices according to the LL-AA model.

In contrast, in most of the HBT-modified devices the low- $T$ /high- $V$  differential conductance  $dI/dV$  vs  $V$  follows a power-law behavior with the same exponents as seen in the corresponding high- $T$ /low- $V$   $G$  vs  $T$  (Figure 1D,  $T \approx 7$  K). Using  $U/\pi\hbar v_F = 6$ ,<sup>26</sup> we found a large increase in the number of channels ( $N = 5–21$ ) and  $l_e$  ( $\approx 35–120$  nm) in our HBT-modified devices, which collectively causes the orders of magnitude enhanced conductance (see Table 1). The large increase of  $l_e$  (or decrease of disorder density,  $L/l_e < 10^2$ ) is clearly a result of defect annealing during the HBT. The increased number of LL channels is expected to drive  $g \rightarrow 0$  and we find  $0.08 \leq g \leq 0.18$ , establishing that the HBT-modified devices are strongly correlated, disordered ( $L/l_e \gg 1$ ), multichannel quantum wires.

Further, the energy scale  $k_B T' = (2\pi\tau'_0/h)^{-1}$  separates the high- $T$  power-law LL, and the low- $T$  AA regimes. We obtain  $T' \approx 187$  K and  $\approx 179$  K for the HBT-1 and HBT-2 device in Figure 1C, respectively. Figure 1E shows the scaling behavior of the renormalized conduc-

tivity  $(\sigma(T)/\sigma_D) \cdot (\tau_0/\tau'_0)$  as a function of the scaled temperature  $T/T'$  (where  $\sigma_D = 2Ne^2 v_F \tau_0/h$  is the Drude conductivity) for different  $G–T$  curves measured on two devices. For comparison, we have digitized the predicted curve from Figure 1 of ref 26 and included it into our Figure 1E. The overlap is quite encouraging, considering such different combinations of  $g$ ,  $N$ , and  $l_e$ , and can be expected to improve further for larger values of  $N$  and a more accurate choice of  $U/\pi\hbar v_F$ . Nevertheless, transport in HBT-modified devices follows the LL-AA picture quite closely. The scaling behavior distinguishes the LL vs AA regimes, with a clear crossover at  $T/T' = 1$ .

The above analysis shows that the HBT process that causes defect annealing and metal-nanocluster decoration in our carbon nanotubes also gives rise to a large enhancement of LL channels. While part of this channel enhancement can be attributed to an access to inner walls mediated by increased long-range graphitization of the nanotubes, it is possible that the presence of metal nanoclusters may also contribute to the increase of quantum channels *via* charge transfer to the nanotubes. It is possible to investigate this in a simpler systems (*e.g.*, in a disorder-free single-wall nanotubes) using *ab initio* density functional theory (DFT) calculations.<sup>27</sup> Our calculations show the appearance of extra electronic bands and enhanced electronic density of states (DoS) near the Fermi level due to surface decoration of single-wall nanotubes using small Pt nanoclusters. Further, calculations based on Landauer formalism and Green's function method using Au contacts confirm enhancement of conductance  $G$  as the Pt atoms are added on the nanotube surface, and these effects can be expected to grow with further Pt coverage of the nanotube surface. Although our calculations are performed for a single-wall nanotube we expect similar behavior for multiwall nanotubes since intershell van der Waal's couplings<sup>6</sup> are weak

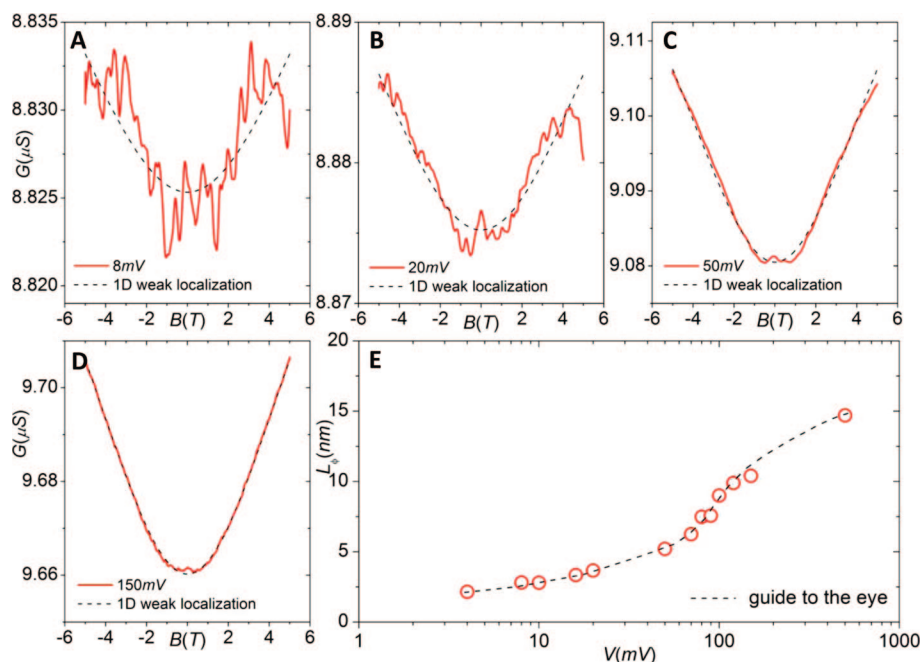


**Figure 2.** (A–D) Magnetoconductance at  $T = 7$  K (measuring bias = 8, 20, 50, and 150 mV). The solid lines are experimental data and the dashed lines are 1D weak-localization model fits. (E) Variation of  $L_\phi$  with bias, calculated from the 1D weak-localization fits.

compared to the Pt-coupling, which is chemical in nature. Hence, we conclude that the Pt-decoration is at least partially responsible for the experimentally observed channel enhancement. As mentioned earlier, access to more walls during the HBT could be another reason for enhanced channels, and we could not independently estimate the individual contributions. However, this does not compromise our analysis of the experimental data.

The HBT-modified devices lie in the crossover region between the “clean” and “strongly disordered” limits. Phase coherence in this regime is expected to be strongly suppressed by  $e-e$  interactions, the dominance of which is itself dependent on the energy of the injected charges. We investigate energy-dependent dephasing by measuring the bias-dependent ( $4 \text{ mV} \leq V \leq 500 \text{ mV}$ ) transverse magnetoconductance (MC) for  $-5 \text{ T} \leq \mathbf{B} \leq 5 \text{ T}$  at  $T \approx 7 \text{ K}$ . Figure 2 panels A–D show the variation of the MC for representative biases. At low energies ( $V < 20 \text{ mV}$ ), the MC shows a number of aperiodic and asymmetric but reproducible oscillations, as shown in Figure 2A. These oscillations were superposed on an overall gradual symmetric increase of MC with increase in  $\mathbf{B}$ , and may be an outcome of DoS singularities in our multichannel quantum wires.<sup>28</sup>

For  $V \geq 20 \text{ mV}$ , the oscillations were significantly suppressed, and we find a small but distinct *negative* MC ( $G(\mathbf{B}) < G(0)$ ) below  $|\mathbf{B}| \approx 0.5 \text{ T}$ , followed by a nearly symmetric and monotonically increasing positive MC all the way up to  $|\mathbf{B}| = 5 \text{ T}$ . This is shown for representative curves in Figures 2B–D. The sub-

stantially larger positive MC can be attributed to the usually observed weak localization in MWNTs,<sup>13</sup> the relative amplitude of which increases with increasing applied bias. Negative magnetoconductance in condensed matter systems is often attributed to strong spin–orbit coupling<sup>29</sup> and is usually absent in bare carbon nanotubes. However, strong  $e-e$  interactions in reduced dimensions and in the presence of disorder and/or heavy adatom clusters on the surface of MWNTs have been very recently predicted to give rise to significant Rashba SO coupling.<sup>18</sup> We believe that the negative MC observed in the heavy atom ( $Z_{\text{Pt}} = 78$ )-nanocluster-decorated MWNTs at low magnetic fields is a signature of Rashba SO coupling. At higher biases, the MC follows a

1D weak localization (WL) correction to conductance,

$$G_{\text{WL}} = G_{\text{D}} - \frac{e^2}{\pi\hbar L} \left\{ L_\phi^{-2} + \frac{(We\mathbf{B})^2}{3\hbar^2} \right\}^{-1/2}$$

Here,  $G_{\text{D}}$  is the Drude conductance ( $=\sigma_{\text{D}}/L$ ) and  $W$  is the effective width of each conducting channel. Figure 2 panels A–D also show attempted WL fits for the data. The fit at the highest bias ( $V = 500 \text{ mV}$ , where WL dominates the most) gives  $G_{\text{D}} \approx 1.11 \times 10^{-5} \text{ S}$ , in excellent agreement with the value ( $\approx 1.14 \times 10^{-5} \text{ S}$ ) independently obtained from LL-AA analysis of  $G$  vs  $T$ . This also establishes that application of higher bias did not access more number of channels compared to the low-bias measurements, implying that the low-bias decoherence is completely energy-driven and not “channel-number” driven. Further, we found a strong dependence of  $L_\phi$  on the applied bias, as shown in Figure 2E. Application of high electric fields is expected to destroy coherence, and hence decrease  $L_\phi$ . In contrast, we find that  $L_\phi$  increases with increasing bias, signifying a lowering impact of  $e-e$  interactions at higher energies in our devices. At low energies, the dominance of  $e-e$  interactions and the destruction of coherent transport are brought out by the almost an order of magnitude suppression of  $L_\phi$ . The low-energy values of  $L_\phi$  ( $\sim 2-3 \text{ nm}$ ) are significantly smaller than  $l_e$  ( $\sim 100 \text{ nm}$ ), indicating that low-energy transport in our disordered multichannel LLs is classically diffusive at the measured temperatures. We note that  $Nl_e$  is between  $0.5-1 \mu\text{m}$  for our most conducting devices, which implies that

short devices with  $L \approx 100$ s of nm can remain quantum mechanically diffusive<sup>10</sup> even at  $T = 0$  K.

To summarize, we have fabricated a new kind of conductance tunable hybrid 1D nanostructure comprising metal nanocluster decorated carbon nanotubes. Transport in these systems undergoes an unprecedented transition from a Luttinger liquid to an Altshuler–Aronov regime, providing the first experimental evidence of the recent theory by Mora *et al.*<sup>10,26</sup> Experimental analysis reveals that these structures have increased number of quantum channels and decreased disorder density compared to pristine nanotubes, possibly due to improved long-range graphitization during the HBT process. The increase in quantum channels can also be partially attributed to charge transfer to the

host nanotube from the metal nanoclusters. This novel system displays rich physics, including the anomalous *increase of phase coherence* with electronic energies arising from the energy-dependent impact of interaction on decoherence, and signature of Rashba spin–orbit scattering in agreement with a recent theoretical prediction. These results open up new avenues for field-theoretical, computational, and experimental research in 1D hybrid structures. The hybrid structures also find tremendous potential applications in the areas of low-resistance nanoelectronic circuitry,<sup>30</sup> fuel cell research,<sup>31</sup> and biosensing.<sup>32</sup> Further, the *in situ* surface decoration technique can be extended to fabricate other new generations of 1D and 2D hybrid nanomaterials.

## MATERIALS AND METHODS

**Device Fabrication.** Multiwall nanotubes were grown inside nanoporous alumina templates by a chemical vapor deposition technique with acetylene ( $C_2H_2$ ) precursor gas at a temperature of approximately 650 °C. CNTs grown in template are uniform in size (~250 nm). This type of growth does not require any separate catalyst sites. The combination of relatively low temperature of growth and absence of catalysts causes these nanotubes to have much less long-range graphitic order, and are characterized by a large amount of structural disorder compared to, for example, arc-discharge produced nanotubes. A NaOH-based etching solution (2–5% mol wt) is used to dissolve the template, a process that leaves behind individual and well-separated tubes. Then MWNTs are dispersed in isopropyl alcohol, sonicated for ~20 min, and spin-cast on a Si/SiO<sub>2</sub> substrate lithographically prepatterned with larger contact pads of Au/Ti. Focus ion beam (FIB) assisted deposition is used to fabricate platinum electrodes connecting the nanotubes to the contact pads. The wafer piece is then mounted onto a chip-holder and the contact pads are wire-bonded to external leads. The chip-holder gets directly mounted onto the cold stage of a cryostat.

**Acknowledgment.** We acknowledge financial support from the Interconnect Focus Center New York at RPI, one of the five Focus Center Research Programs of the Semiconductor Research Corporation (SRC). S.K. also thanks SRC for a Cross-disciplinary Semiconductor Research Fund (2008–2009), and S.T. acknowledges the financial support provided by SIUC through faculty start-up funds.

**Supporting Information Available:** Experimental details on the platinum decoration of MWNTs using “High bias treatment”. This material is available free of charge via the Internet at <http://pubs.acs.org>.

## REFERENCES AND NOTES

- Kane, C.; Balents, L.; Fisher, M. P. A. Coulomb Interactions and Mesoscopic Effects in Carbon Nanotubes. *Phys. Rev. Lett.* **1997**, *79*, 5086–5089.
- Giamarchi, T.; Schultz, H. J. Anderson Localization and Interactions in One-Dimensional Metals. *Phys. Rev. B* **1988**, *37*, 325–340.
- Chang, A. M.; Pfeiffer, L. N.; West, K. W. Observation of Chiral Luttinger Behavior in Electron Tunneling into Fractional Quantum Hall Edges. *Phys. Rev. Lett.* **1996**, *77*, 2538–2541.
- Venkataraman, L.; Hong, Y. S.; Kim, P. Electron Transport in a Multichannel One-Dimensional Conductor: Molybdenum Selenide Nanowires. *Phys. Rev. Lett.* **2006**, *96*, 076601-1–076601-4.
- Yao, Z.; Postma, H. W. Ch.; Balents, L.; Dekker, C. Carbon Nanotube Intramolecular Junctions. *Nature* **1999**, *402*, 273–276.
- Charlier, J.-C.; Blase, X.; Roche, S. Electronic and Transport Properties of Nanotubes. *Rev. Mod. Phys.* **2007**, *79*, 677–732.
- Bockrath, M.; Cobden, D. H.; Lu, J.; Rinzler, A. G.; Smalley, R. E.; Balents, L.; McEuen, P. L. Luttinger-Liquid Behaviour in Carbon Nanotubes. *Nature* **1999**, *397*, 598–601.
- Langer, L.; Bayot, V.; Grivei, E.; Issi, J.-P.; Heremans, J. P.; Olk, C. H.; Stockman, L.; van Haesendonck, C.; Bruynseraede, Y. Quantum Transport in a Multiwalled Carbon Nanotube. *Phys. Rev. Lett.* **1996**, *76*, 479–482.
- Schönenberger, C.; Bachtold, A.; Strunk, C.; Salvétat, J.-P.; Forró, L. Interference and Interaction in Multi-Wall Carbon Nanotubes. *Appl. Phys. A* **1999**, *69*, 283–295.
- Mora, C.; Egger, R.; Altland, A. From Luttinger Liquid to Altshuler–Aronov Anomaly in Multichannel Quantum Wires. *Phys. Rev. B* **2007**, *75*, 035310-1–035310-14.
- Altshuler, B. L.; Aronov, A. G. *Electron-Electron Interactions in Disordered Systems*; Efros, A. L., Pollak, M., Eds.; North-Holland: Amsterdam, The Netherlands, 1985.
- Stojetz, B.; Miko, C.; Forró, L.; Strunk, C. Effect of Band Structure on Quantum Interference in Multiwall Carbon Nanotubes. *Phys. Rev. Lett.* **2005**, *94*, 186802-1–186802-4.
- Krompiewski, S.; Dugaev, V. K.; Barnaś, J. Resonant Decoherence Due to Electron-Electron Interactions in Carbon Nanotubes. *Phys. Rev. B* **2007**, *75*, 195422-1–195422-5.
- Davydov, D. N.; Li, J.; Shelimov, K. B.; Haslett, T. L.; Moskovits, M. Resistance and Tunneling Spectra of Aligned Multiwalled Carbon Nanotube Arrays. *J. App. Phys.* **2000**, *88*, 7205–7208.
- Jang, W. Y.; Kulkarni, N. N.; Shih, C.; Yao, Z. Electrical Characterization of Individual Carbon Nanotubes Grown in Nanoporous Anodic Alumina Templates. *Appl. Phys. Lett.* **2004**, *84*, 1177–1179.
- Skákalová, V.; Kaiser, A. B.; Woo, Y.-S.; Roth, S. Electronic Transport in Carbon Nanotubes: From Individual Nanotubes to Thin and Thick Networks. *Phys. Rev. B* **2006**, *74*, 085403-1–085403-10.
- Xu, F.; Li, B.; Pan, H.; Zhu, J.-L. Spin-Orbit Coupling Effects on Transport in Carbon Nanotubes with Adatoms. *Phys. Rev. B* **2007**, *75*, 085431-1–085431-6.
- See Supporting Information for detailed experimental method and related observations.
- Chen, S.; Huang, J. Y.; Wang, Z.; Kempa, K.; Chen, G.; Ren, Z. F. High-Bias-Induced Structure and the Corresponding Electronic Property Changes in Carbon Nanotubes. *Appl. Phys. Lett.* **2005**, *87*, 263107-1–263107-3.

20. Papadopoulos, C.; Rakitin, A.; Li, J.; Vedenev, A. S.; Xu, J. M. Electronic Transport in Y-Junction Carbon Nanotubes. *Phys. Rev. Lett.* **2000**, *85*, 3476–3479.
21. Tarkiainen, R.; Ahlskog, M.; Zyuzin, A.; Hakonen, P.; Paalanen, M. Transport in Strongly Disordered Multiwalled Carbon Nanotubes. *Phys. Rev. B* **2004**, *69*, 033402-1–033402-4.
22. Tarkiainen, R.; Ahlskog, M.; Penttila, J.; Roschier, L.; Hakonen, P.; Paalanen, M.; Sonin, E. Multiwalled Carbon Nanotube: Luttinger versus Fermi Liquid. *Phys. Rev. B* **2001**, *64*, 195412-1–195412-4.
23. Gornyi, I. V.; Mirlin, A. D.; Polyakov, D. G. Dephasing and Weak Localization in Disordered Luttinger Liquid. *Phys. Rev. Lett.* **2005**, *95*, 046404-1–046404-4.
24. Tsai, M.-Y.; Yu, C.-Y.; Yang, C.-H.; Tai, N.-H.; Perng, T.-P.; Tu, C.-M.; Husain Kan, Z.; Liao, Y.-C.; Chi, C. C. Electrical Transport Properties of Individual Disordered Multiwalled Carbon Nanotubes. *Appl. Phys. Lett.* **2006**, *89*, 192115-1–192115-3.
25. Cho, Y. S.; Song, I. K.; Hong, S.-K.; Im, W. S.; Choi, G. S.; Kim, D. Synthesis Mechanism of Flaked Carbon Nanotubes Formed on an Anodic Aluminum Oxide Template Examined via Transmission Electron Microscopy. *J. Kor. Phys. Soc.* **2005**, *47*, 344–347.
26. Mora, C.; Egger, R.; Altland, A. Interaction Correction to the Conductivity of Disordered Multi-Wall Carbon Nanotubes. *Semicond. Sci. Technol.* **2006**, *21*, S46–S51.
27. Parr, R. G.; Yang, W. *Density-Functional Theory of Atoms and Molecules*; Oxford University Press: Oxford, U.K., 1989. Details of our DFT calculations will be published elsewhere.
28. Tserkovnyak, Y.; Halperin, B. I. Magnetoconductance Oscillations in Quasiballistic Multimode Nanowires. *Phys. Rev. B* **2006**, *74*, 245327-1–245327-10.
29. Bergmann, G. Weak Localization in Thin Films: a Time-of-Flight Experiment with Conduction Electrons. *Phys. Rep.* **1984**, *107*, 1–58.
30. Naeemi, A.; Sarvari, R.; Meindl, J. D. Performance Comparison Between Carbon Nanotube and Copper Interconnects for Gigascale Integration (GSI). *IEEE Electron Device Lett.* **2005**, *26*, 84–86.
31. Selvaraj, V.; Alagar, M. Pt and Pt–Ru Nanoparticles Decorated Polypyrrole/Multiwalled Carbon Nanotubes and Their Catalytic Activity Towards Methanol Oxidation. *Electrochem. Commun.* **2007**, *9*, 1145–1153.
32. Qiaocui, S.; Tuzhi, P.; Yunu, Z.; Yang, C. F. An Electrochemical Biosensor with Cholesterol Oxidase/Sol-Gel Film on a Nanoplatinum/Carbon Nanotube Electrode. *Electroanal.* **2005**, *17*, 857–861.